Investigation of physicochemical and electrical properties of TiO_2 nanotubes/graphene oxide nanocomposite

MARWA HAMANDI[1], MOHAMED TRIKI[2,*], JORDI LLORCA[3], FETHI JOMNI[4], NUHAD A ALOMAIR[5,6] and HAFEDH KOCHKAR[5,6]

[1] Université de Tunis El Manar, Laboratoire de Chimie des Matériaux et Catalyse (LCMC), Faculté des Sciences de Tunis, 2092 El Manar, Tunisia

[2] Centre National des Recherches en Sciences des Matériaux, Laboratoire de Valorisation des Matériaux Utiles (LVMU), Pôle Technologique Borj Cedria, 8027 Soliman, Tunisia

[3] Institute of Energy Technologies, Department of Chemical Engineering and Barcelona Research Center in Multiscale Science and Engineering, Universitat Politècnica de Catalunya, EEBE, Eduard Maristany 16, 08019 Barcelona, Spain

[4] Université de Tunis El Manar, Laboratoire Matériaux Organisation et Propriétés (LR99ES17), Faculté des Sciences de Tunis, 2092 El Manar, Tunisia

[5] Imam Abdulrahman Bin Faisal University, College of Science, P.O. Box 1982, 31441, Dammam, Saudi Arabia

[6] Basic & Applied Scientific Research Center, Imam Abdulrahman Bin Faisal University, P.O. Box 1982, 31441, Dammam, Saudi Arabia

[*] Author for correspondence (mhtriki@gmail.com)

Abstract. GO/HNT400 nanocomposite was prepared by incipient impregnation of TiO_2 nanotubes (HNT400) with graphene oxide (GO) dispersion. GO was elaborated by an improved Hummer's method while HNT400 was obtained using alkaline hydrothermal treatment of TiO_2 P25 followed by calcination at 400°C. Raman results showed the characteristic bands of GO in addition to anatase. TEM analysis confirmed the formation of GO nanosheets assembled to TiO_2 nanotubes. XRD analysis showed that GO nanosheets do not change neither the structural nor the morphological properties of TiO_2 nanotubes. XPS and EPR measurements confirmed the electron transfer between GO and TiO_2 nanotubes. PL analysis revealed that GO inhibits the recombination of photogenerated electron-hole pairs in

the GO/HNT400 nanocomposite. The ac conductivity measurements suggested the presence of bulk and grain boundary effect in the nanocomposite.

Keywords. Graphene oxide; TiO_2 nanotubes; Electronic effect; Grain boundary.

1. Introduction

Graphene oxide (GO) has received tremendous attention since it was identified as graphene precursor [1]. It is an environmentally friendly and cheap material, which permits to open different routes for several promising applications. GO has been described in many recent reviews as potential material due to its high surface area, conductivity, good interfacial surface and easy synthesis process [2, 3]. GO has been synthesized by a variety of methods, among them, the Hummer's method based on the chemical exfoliation of graphite using $KMnO_4$ as oxidizing agent [4]. This oxidation method was found to form functional groups (carboxyl, hydroxyl and epoxy) on the surface of GO nanosheets, which facilitate surface tuning [5, 6]. Therefore, a deep understanding of its electronic properties, especially when it is in the nanocomposite form, is an important target [7]. Synergistic effects due to the interface modification on the charge transport in graphene hybrid systems have been reported in a variety of applications, such as catalysis [8], photocatalysis [9, 10], transparent conductors [11], sensors and energy conversion [12]. Particularly, the hybridization of TiO_2 with graphene can significantly tune the energy bandgap. Due to this hybridization, the absorption threshold shifts from the UV to the edge of the visible range [13]. Nanocomposites based on TiO_2 and GO have been investigated in many applications such as lithium ion batteries, photocatalysis and energy-related fields [14], dye-sensitized solar cells [15] and sensing process [16]. Especially, TiO_2 nanotubes wrapped with reduced graphene oxide (rGO) were used as a high performance anode material for lithium ion batteries [17], for gas sensing [18]

and for electrical double layer capacitors [19]. Many synthesis methods of GO/TiO_2 nanocomposite have been described in the literature such as sol-gel, hydrothermal, mixing and/or sonication, and electrochemical processes [20]. It has been reported that GO/TiO_2 and rGO-decorated TiO_2 nanocomposites lead to the improvement of both visible light absorption and electron-hole pair separation [21, 22]. However, the heterojunction of GO in nanocomposites is still controversial [23]. In addition, the electronic interaction between graphene oxide and TiO_2 nanotubes is not fully understood and remains a challenge due to the compact (bunched) morphology of the nanotubes.

Herein, we have prepared the GO/TiO_2 nanotubes nanocomposite by simple impregnation. The nanocomposite is deeply characterized by XRD, Raman, TEM, XPS, EPR, and photoluminescence and compared to pure GO and TiO_2 nanotubes. The frequency and temperature dependence of the electrical conductivity is also discussed.

2. Materials and methods

2.1 *Preparation of materials*

The improved Hummer's method was used to prepare graphene oxide as described previously [24]. Graphite (3.0 g) was added to 70 mL of H_2SO_4/H_3PO_4 (9/1 v/v) under stirring in an ice bath. After addition of $KMnO_4$ (9.0 g), the suspension was kept under stirring for 30 min. Then, water (150 mL) was added and the suspension was stirred for 15 min at 40°C. After a slowly addition of H_2O_2 (15 mL), the mixture was filtered and washed with 250 mL of HCl (0.1 M). The obtained material was mixed with water (600 mL) to obtain a graphite oxide dispersion, which was sonicated for 6 hours and stirred overnight. The dispersion was finally centrifuged at 10000 rpm for 30 min to obtain graphene oxide labeled as GO. TiO_2 nanotubes were prepared using the alkaline hydrothermal method described previously [25]. TiO_2 P25 (3.0 g) were treated with 90 mL of NaOH (11.25 mol L^{-1}) in a Teflon-lined autoclave at

130°C for 20 h. After filtration, washing with HCl solutions (0.1 and 1.0 mol L^{-1}) and water, the material was calcined at 400°C under air for 2 h and labeled as HNT400. The nanocomposite was prepared by incipient impregnation of HNT400 with the GO dispersion. The GO content in the nanocomposite was fixed at 10 wt%. The mixture was dried at 80°C for 24 h and labeled as GO/HNT400.

2.2 *Materials characterization*

X-ray diffraction analyses were determined by Panalytical, X'Pert Pro apparatus using Cu*Kα* radiation. Raman spectra were recorded with a Micro-Raman instrument TG 4000 (IVAN) using a He-Ne laser as incident light (488 nm). FTIR spectra were recorded using a Bruker Vertex 70 spectrometer in attenuated total reflectance mode. Photoluminescence (PL) analysis was performed on a PerkinElmer LS55 spectrofluophotometer equipped with a Xe lamp. The excitation wavelength was 330 nm. Transmission electron microscopy (TEM) was operated by a JEOL JEM-1011 instrument operating at 200 kV. Surface characterization was done with X-ray photoelectron spectroscopy (XPS) on a SPECS system equipped with an Al anode XR50 source operating at 150 W and a Phoibos 150 MCD-9 detector. Data processing was performed with the Casa XPS program and the binding energy (BE) values were referred to the C1s peak at 284.8 eV. Electron paramagnetic resonance (EPR) spectra were recorded at room temperature on a Bruker ER-200D spectrometer (9.3 GHz). Electrical conductivity measurements were studied in air on a cylindrical pellet with a diameter of 13 mm, a thickness of 3 mm and a relative density of about 92%. The electrical ac conductivity was performed by a Frequency Response Analyzer Solartron 1260A coupled with 1296A dielectric interface in frequency domain of 0.1-10^6 Hz and temperature range of 25-300°C. The Nyquist curves, imaginary part (-Z") *versus* real part (Z'), were plotted with Origin 8 software (Microcal Software, Inc., Northampton, Ma USA). The ac conductivity (σ_{ac}) was deduced using the following equation:

$\sigma_{ac} = \omega\varepsilon_0\varepsilon''$

where ω is the angular frequency of applied field, ε_0 is the free space permittivity and ε'' is the dielectric loss determined from Z' and Z".

3. Results and discussion

The textural analyses show that HNT400 and GO/HNT400 present an isotherm of type-IV and a H3 hysteresis in favor of the presence of mesopores (*Figure S1, Supplementary information*). The impregnation with graphene oxide did not significantly modify the BET surface area of HNT400. The specific surface area is 178 $m^2 g^{-1}$ for HNT400 against 166 $m^2 g^{-1}$ for GO/HNT400. On the contrary, a decrease in the pore volume is observed, 0.56 vs. 0.37 $cm^3 g^{-1}$ for HNT400 and GO/HNT400, respectively (*Figure S2, Supplementary information*). This is ascribed to a strong interaction between the two components of the nanocomposite material. The XRD pattern of GO/HNT400 (Figure 1a) shows peaks at 25.4°, 38.1°, 48.3°, 54.0°, 55.1° and 62.8° corresponding to the anatase phase (JCPDS 21-1272). This result indicates that GO nanosheets do not change the structure of HNT400. The conversion of graphite to GO is identified by the appearance of new peak at 10.8° known as a fingerprint of GO (Figure 1c). On the other hand, GO does not produce any sharp XRD peak because the oxidation treatment destroys the initial (002) peak of pristine graphite (Figure 1b), thus making the resulting GO like amorphous material [26]. In addition, during the oxidation process, the interlayer distance increases from 3.4 to 8.3 Å because of the incorporation of water and oxygen functional groups [27].

Figure 1.

According to thermal analysis of GO/HNT400 (*Figure S3b, Supplementary information*), there are three obvious steps of mass loss. A first mass loss of 2.2% at 100°C corresponding to the loss of physisorbed water; a second mass loss of 4.2% at 200°C assigned to the desorption of the structural water; and a third mass loss of 5.4% at 500°C probably due to the

decomposition of labile oxygen functional groups of GO [28]. The exothermic peak at about 750°C could be assigned to the phase change from anatase to rutile. This phase change takes place at 600°C in the case of HNT400 as shown in *Figure S3a (Supplementary information*). This can be explained due to the fact that GO nanosheets stabilize the anatase phase up to 750°C. Figure 2 shows the Raman spectra of GO and GO/HNT400. The Raman spectrum of GO shows the presence of the D and G bands, characteristic of graphene oxide, around 1372 and 1618 cm^{-1}, respectively. The G band offers information about the vibration in the plane of the sp^2 bonds of the carbon atoms [29]. As for the D band, it informs about the presence of the sp^3 bonds and structural defects in GO [30]. Thus, the presence of these bands indicates the formation of graphene oxide as shown previously [31]. Compared to GO, the Raman spectrum of GO/HNT400 exhibits the D and G bands with a slightly blue shift and lower intensity. The shift from 1618 to 1602 cm^{-1} observed for the G band is explained by the presence of isolated double bonds, which tend to resonate at high frequency compared to the G band of graphite [32, 33]. On the other hand, the GO/HNT400 nanocomposite shows a slight increase in the calculated (I_D/I_G) ratio (0.865) compared to GO (0.847), indicating a lower density of defects in GO. In addition, the Raman spectrum of GO/HNT400 shows characteristic bands at 146 (E_g), 393 (B_{1g}), 511 (B_{2g}) and 638 cm^{-1} (E_g) ascribed to anatase as reported in *Figure S4 (Supplementary information*). These results confirm the formation of the TiO_2 nanotubes-GO assemblage, in agreement with XRD results.

Figure 2.

Figure 3 shows the FTIR spectra of GO, HNT400 and GO/HNT400. The spectrum of GO presents several bands corresponding to oxygen groups on the surface and edges of each plane of GO. Indeed, the bands at 1658 and 3420 cm^{-1} are attributed to isolated hydroxyl groups (–OH) of intercalated water in GO. Moreover, the bands at 1100 and 1160 cm^{-1} correspond to stretching vibration (C–O and C–O–C) of the alkoxy and epoxy groups, respectively. The

bands at 1410 and 1735 cm^{-1} are attributed to stretching vibrations (C–OH and C=O) of the carboxyl group, which is in accordance with the oxidation of graphite to graphene oxide as shown previously [34, 35]. In GO/HNT400 the band at 1710 cm^{-1} disappears, which confirms the interaction between –OH groups of TiO_2 nanotubes and graphene oxide.

Figure 3.

XPS spectra of GO and GO/HNT400 are shown in Figure 4. For the GO sample, the C 1s spectrum contains mainly three signals at 284.7, 286.9 and 288.5 eV. The binding energy at 284.7 eV could be assigned to the C–C bond (sp^2) of graphene [36]. The binding energies at 286.9 and 288.5 eV are ascribed to the C−O and C=O bonds, respectively [37, 38]. The O 1s spectrum of GO (*Figure S5, Supplementary information*) also suggests the existence of C–O bond, indicating the presence of defects in GO [39]. Interestingly, the spectrum of C1s of GO/HNT400 shows a remarkable decrease in the carbon-oxygen species since the signal at 286.9 eV is less intense compared to GO. This result confirms the existence of a strong interaction between –OH groups of graphene oxide and TiO_2 nanotubes, in agreement with FTIR results. The signal of Ti 2p (*Figure S6, Supporting information*) indicates that Ti is in the form of TiO_2 and the atomic surface ratio of GO and TiO_2 calculated from the C 1s and Ti 2p lines is GO:TiO_2=1.2 .

Figure 4.

The morphological properties of GO and GO/HNT400 are investigated by TEM and the micrographs are shown in Figure 5. Figure 5a shows the characteristic layered structure of GO. GO/HNT400 shows multilayer graphene oxide nanosheets wrapping TiO_2 nanotubes with a diameter of 10-14 nm and a wall thickness of 2-3 nm (Figure 5b). Therefore, the close contact between GO and TiO_2 nanotubes is confirmed, in accordance with the information provided with the characterization methods discussed above.

Figure 5.

EPR spectra of HNT400, GO and GO/HNT400 are shown in Figure 6. The EPR spectrum of HNT400 (Figure 6a) contains a weak signal at g=1.99, suggesting the existence of oxygen vacancies at the surface of TiO_2 nanotubes [40]. In the EPR spectrum of GO (Figure 6c), a well-defined g=2.0036 component is observed, which is close to the free electron g-value of g_e=2.0023. This result is characteristic of localized defects spins, which is in good agreement with previous reports [41]. The EPR spectrum of GO/HNT400 (Figure 6b) shows the same feature at g=2.0036 but with lower intensity (half), which confirms the modification of GO nanosheets with TiO_2 nanotubes in agreement with XPS analysis. In addition, the signal at g=1.99 could be partially hidden by the intense signal at g=2.0036. Therefore, changes in EPR spectra again confirmed the close interaction between TiO_2 nanotubes and the surface of GO nanosheets. This highlights the role of defects and oxygen functionalities in the spin localization phenomena especially for the GO/HNT400 nanocomposite.

Figure 6.

PL emission spectra of HNT400 and GO/HNT400 with excitation wavelength at 330 nm are reported in Figure 7. The PL spectrum of HNT400 (Figure 7a) shows a strong peak at 386 nm due to the recombination of photoexcited electron-hole pairs and corresponding to the band-gap energy of anatase (3.21 eV). The broad emission peaks at 434 and 481 nm could be assigned to indirect band edge and reveal the presence of surface oxygen vacancies and defects due to self-trapped excitons [42]. For, the green emission peak at 528 nm, it could be defined as surface state emissions, whereas the charge carriers could be trapped by oxygen vacancies and contribute to visible luminescence [43]. However, the introduction of GO decreases the PL emission intensity of TiO_2 nanotubes as shown in the PL spectrum of GO/HNT400 (Figure 7b). In fact, the emission peaks were significantly quenched while the main emission of origin material was not changed, which points out to a charge recombination reduction in agreement with previous studies [44, 45]. In fact, the electrons are likely excited

from VB to CB and then transferred to GO nanosheets inhibiting the recombination rate of photo-induced electrons and holes in GO/HNT400 [46-48], which is consistent with EPR analyses.

Figure 7.

Regarding the ac conductivity measurements, the following empirical equation [49] has been used to describe the overall ac conductivity:

$$\sigma_{ac}(\omega) = \sigma_i\,(T) + k_1(T)\omega^{\alpha 1} + \sigma_b(T) + k_2(T)\,\omega^{\alpha 2} \quad (1)$$

where T is the absolute temperature, ω is the angular frequency, k_1 and k_2 are two constants, σ_i and σ_b correspond to the interfacial and bulk conductivities, respectively. Figure 8 shows the frequency variation of ac conductivity at various temperatures. For T < 200°C, the ac conductivity shows a first plateau at low frequencies, which corresponds to the frequency-independent dc conductivity (σ_i). This behavior can be attributed to electrode polarization effects of the long range hopping of mobile ions (oxygen vacancies). At high frequencies, the ac conductivity varies as a power law with frequency ($k_1\omega^{\alpha 1}$). This is a typical behavior of an ac conduction dominated by a short-range hopping process with a distribution of energy barriers. For T > 200°C, the ac conductivity shows the same behavior at low and mid frequencies. In addition, at higher temperature, the ac conductivity exhibits a second plateau (σ_b). This is probably attributed to the detrapping of active sites between TiO_2 nanotubes and graphene oxide due to the thermally activated process. The thermal activation energies (Ea) for the low and high frequency plateaus were estimated on the basis of Arrhenius plots (*Figure S7, Supporting information*). The corresponding values Ea were about 0.23 and 0.28 eV at 0.15 Hz and 54 kHz, respectively. These values are comparable with other forms of TiO_2 structures [50].

Figure 8.

Figure 9 shows the Nyquist plots of GO/HNT400 at 200 and 250°C. The effect of temperature on the impedance of the material is noticeable. For T=200°C, two semicircles are plotted. The low frequency arc is attributed to the polarization in the grain boundaries, whereas the high frequency arc is attributed to the polarization in the grain [51]. As temperature increases, the grain and the grain boundaries resistances decrease, which is in agreement with the thermally activated conduction in the GO/HNT400 nanocomposite.

Figure 9.

4. Conclusions

In this work, an intimate contact between graphene oxide (GO) and TiO_2 nanotubes (HNT400) in nanocomposites prepared by simple impregnation has been demonstrated. The GO/HNT400 nanocomposite shows a strong suppression of the recombination of photogenerated electron-hole pairs in TiO_2 nanotubes due to the electron acceptor characteristics of graphene oxide.

Acknowledgements

The authors gratefully acknowledge the help of Pr. Faouzi Hosni from CNSTN (Tunisia) for EPR measurements.

References

[1] Li F, Jiang B X, Zhao C J and Zhang S 2015 *Nano Energy* **16** 488

[2] Low F W, Lai C W 2018 *Renew. Sust. Energ. Rev.***82** 103

[3] Tian P, Tang L, Teng K S and Lau S P 2018 *Mater. Today Chem.***10** 221

[4] Hummers W S and Offeman R E 1958 *J. Am. Chem. Soc.* **80** 1339

[5] He H, Klinowski J, Forster M and Lerf A 1998 *Chem. Phys. Lett.* **287** 53

[6] Muszynski R, Seger B and Kamat P V 2008 *J. Phys. Chem. C* **112** 5263

[7] Rao C N R, Sood A K, Subrahmanyam K S and Govindaraj A 2009 *Angew. Chem. Int. Ed.* **48** 7752

[8] Szczęśniak B, Choma J and Jaroniec M 2018 *J Colloid Interface Sci.* **514** 801

[9] Nguyen C H, Juang R S 2019 *J. Ind. Eng. Chem.***76** 296

[10] Chen L, Yang S, Mu L and Ma P C 2018 *J. Colloid Interface Sci.* **512** 647

[11] Sohna H, Woo Y S, Shin W *et al* 2017 *Appl. Surf. Sci.* **419** 63

[12] Anju M and Renuka N K 2019 *Nano-Structures & Nano-Objects* **17** 194

[13] Saleem A, Ullah N, Khursheed K*et al* 2018 *J. Electronic Mater.* **47**(7) 3749

[14] Kiarii E M, Govender K K, Ndungu P G and Govender P P 2018 *Bull. Mater. Sci.* **41** 75

[15] Siwach B, Mohan D, Sharma S and Jyoti D 2017 *Bull. Mater. Sci.* **40**(7) 1371

[16] Harraz F A, Faisal M, Ismail A A *et al* 2019 *J. Electroanal. Chem.* **832** 225

[17] Zheng P, Liu T, Su Y *et al* 2016 *Sci. Rep.* **6** 36580

[18] Galstyan V, Ponzoni A, I Kholmanov I *et al* 2018 *ACS Appl. Nano Mater.* **1** 7098

[19] Lazarte J P L, Dipasupil R C, Pasco G Y S *et al* 2018 *Nanomaterials* **8** 934

[20] N T Tho, N T T Mai, N T Van, *et al* 2019 *J. Nanosci. Nanotechnol.* **19** 5195

[21] Chen C, Cai W, Long M *et al* 2010 ACS Nano **4** 6425

[22] Rambabu Y, Jaiswal M and Roy S C 2016 *AIP Adv.* **6** 115010

[23] Rajender G, Kumar J, Giri P K 2018 *Appl. Catal. B* **224** 960

[24] Hamandi M, Berhault G, Guillard C and Kochkar H 2017 *Appl. Catal. B* **209** 203

[25] Triki M, Tanazefti H and Kochkar H 2017 *J. Colloid Interface Sci.* **493** 77

[26] Botas C, Alvarez P, Blanco C *et al* 2012 *Carbon* **50** 275

[27] Sutar D S, Singh G and Botcha D V 2012 *Appl. Phys. Lett.* **101** 103103

[28] Guo J J, Zhu S M, Chen Z X *et al* 2011 *Ultrason. Sonochem.* **18** 1082

[29] Pimenta M A, Dresselhaus G, Dresselhaus M S *et al* 2007 *Phys. Chem. Chem. Phys.* **9** 1276

[30] Zhang W, Cui J, Tao C A *et al* 2009 *Angew. Chem. In. Ed.* **48** 5864

[31] Dreyer D R, Park S, Bielawski C W and Ruoff R S 2010 *Chem. Soc. Rev.* **39** 228

[32] Ramesha G K and Sampath S 2009 *J. Phys. Chem. C* **113**(19) 7985

[33] Yoo E, Okata T, Akita T *et al* 2009 *Nano Lett.* **9**(6) 2255

[34] Stankovich S, Dikin D A, Piner R D *et al* 2007 *Carbon* **45** 1558

[35] Acik M, Mattevi C, Gong C *et al* 2010 *ACS Nano* **4** 5861

[36] Zhou X Z, Huang X, Qi X Y *et al* 2009 *J. Phys. Chem. C* **113** 10842

[37] Hu C, Chen F, Lu T, *et al* 2014 *Mater. Lett.* **121** 209

[38] Rourke J P, Pandey P A, Moore J J *et al* 2011 *Angew. Chem. Int. Ed.* **50** 3173

[39] Wild U, Pfander N and Schlogl R 1997 *Fresenium J. Anal. Chem.* **357** 420

[40] Nakamura I, Negishi N, Kutsuna S *et al* 2000 *J. Mol. Catal. A* **161** 205

[41] Barklie R C 2003 *Diamond Relat. Mater.* **12** 1427

[42] Yu J, Ma T and Liu S 2011 *Phys. Chem. Chem. Phys.* **13** 3491

[43] Aronne A, Fantauzzi M, Imparato C *et al* 2017 *RSC Adv.* **7** 2373

[44] Leary R and Westwood A 2011 *Carbon* **49** 741

[45] Williams G, Seger B and Kamat P V 2008 *ACS Nano* **2** 1487

[46] Sagadevan S, Pal K, Koteeswari P and Subashini A 2017 *J. Mater. Sci.: Mater. Electron.* **28** 7892

[47] Dubey P K, Tripathi P, Tiwari R S *et al* 2014 *Int. J. Hydrogen Energy* **39** 16282

[48] Xiang Q, Yu J and Jaroniec M 2011 *Nanoscale* **3** 3670

[49] Jonscher A K 1983 (first ed) *Dielectric relaxation in solids* (London: Chelsea Dielectrics Press)

[50] Huber B, Brodyanski A, Scheib M *et al* 2005 *Thin Solid Films* **472** 114

[51] Selmi A, Khaldi O, Mascot M *et al* 2016 *J. Mater. Sci.: Mater. Electron.* **27** 11299

Figures captions

Figure 1. XRD patterns of (a) GO/HNT400, (b) graphite and (c) GO.

Figure 2. Raman spectra of (a) GO and (b) GO/HNT400.

Figure 3. FTIR spectra of (a) HNT400, (b) GO/HNT400 and (c) GO.

Figure 4. XPS C1s core level of GO and GO/HNT400.

Figure 5. TEM images of (a) GO and (b) GO/HNT400.

Figure 6. EPR spectra at room temperature (X-band) of (a) HNT400, (b) GO/HNT400 and (c) GO. *Inset shows zoom of the narrow EPR line for GO and GO/HNT400.*

Figure 7. PL emission spectra of (a) HNT400 and (b) GO/HNT400.

Figure 8. Frequency dependence of the ac conductivity from 25 to 300°C.

Figure 9. Nyquist plots of GO/HNT400 at 200 and 250°C.

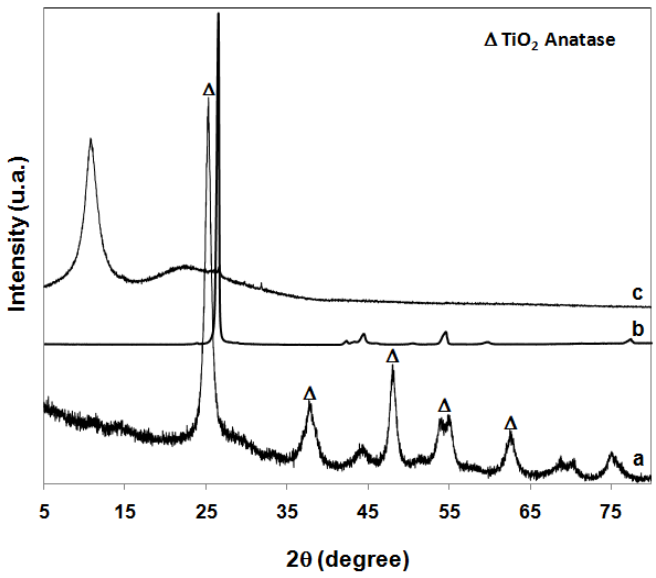

Figure 1.

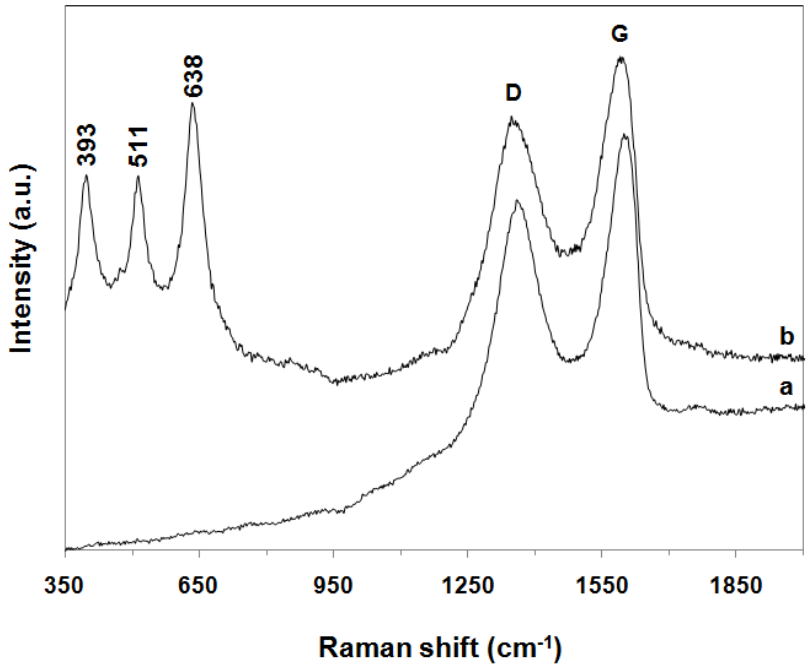

Figure 2.

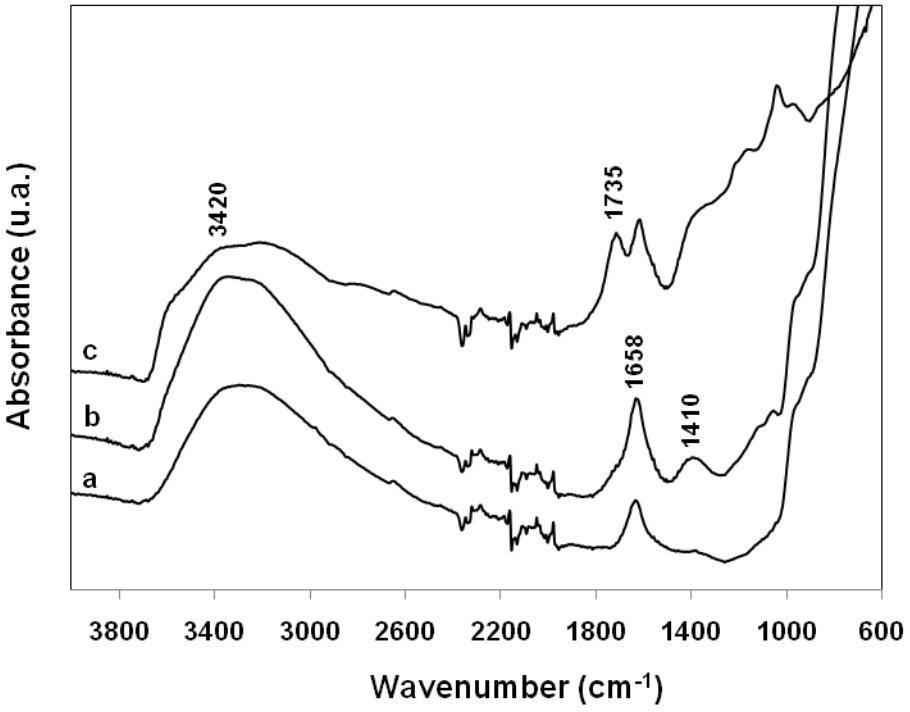

Figure 3.

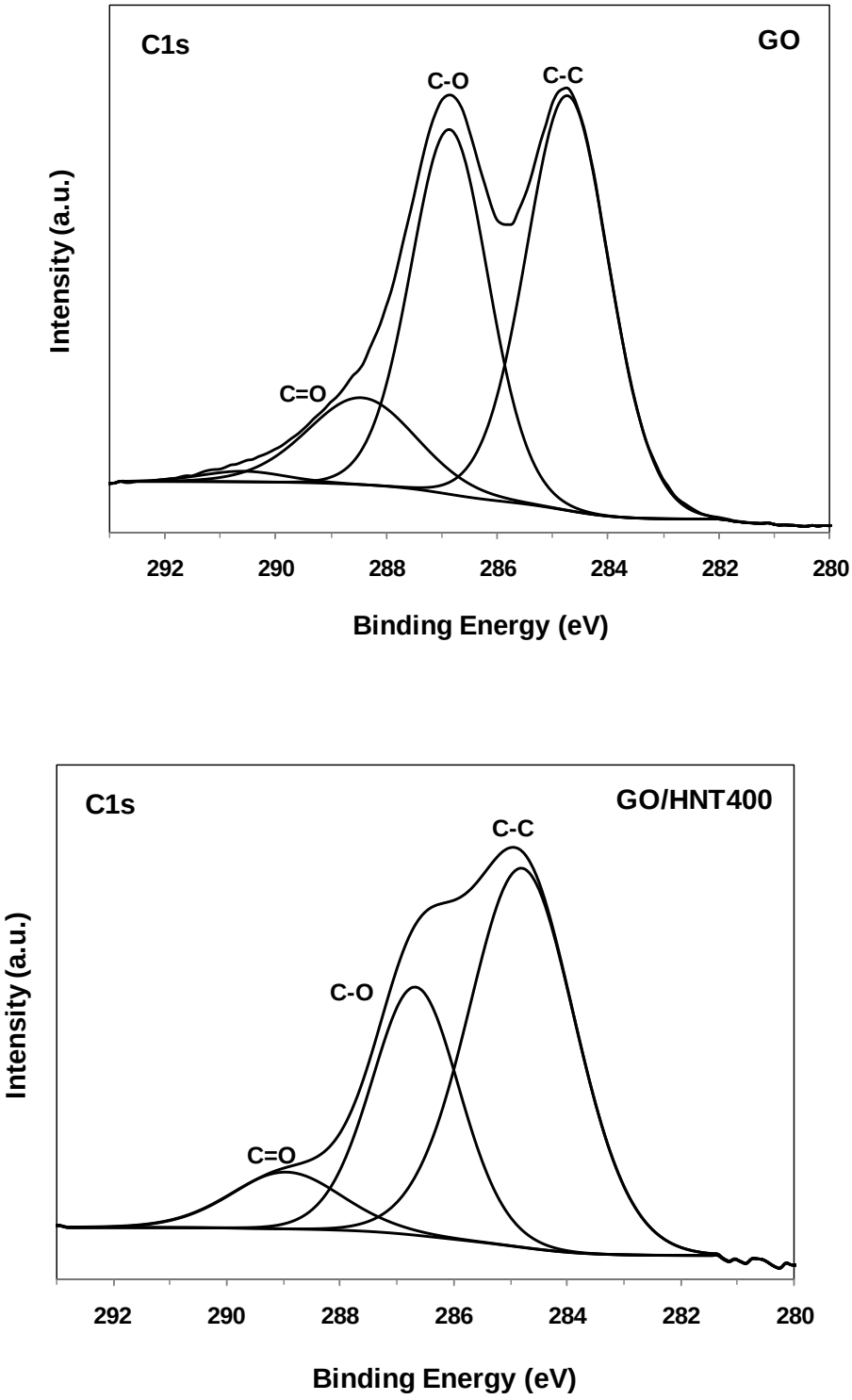
C1s
GO
C-O
C-C
C=O
Intensity (a.u.)
292
290
288
286
284
282
280
Binding Energy (eV)
C1s
GO/HNT400
C-C
C-O
C=O
Intensity (a.u.)
292
290
288
286
284
282
280
Binding Energy (eV)

Figure 4.

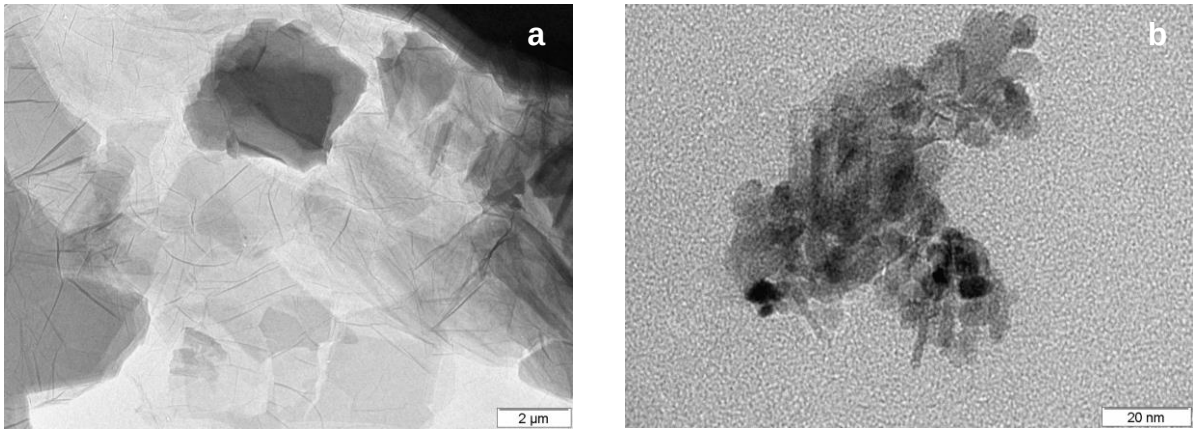

Figure 5.

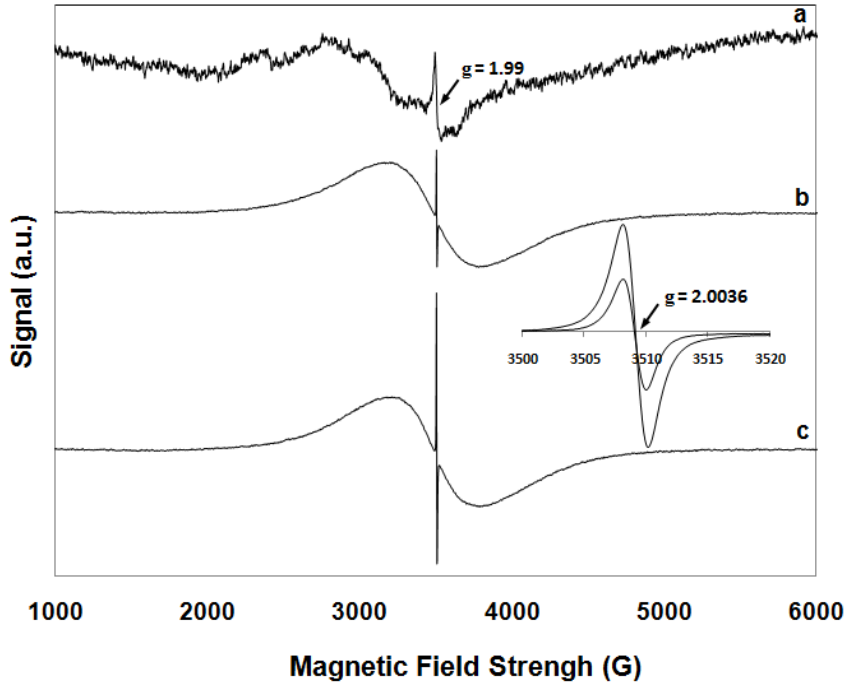

Figure 6.

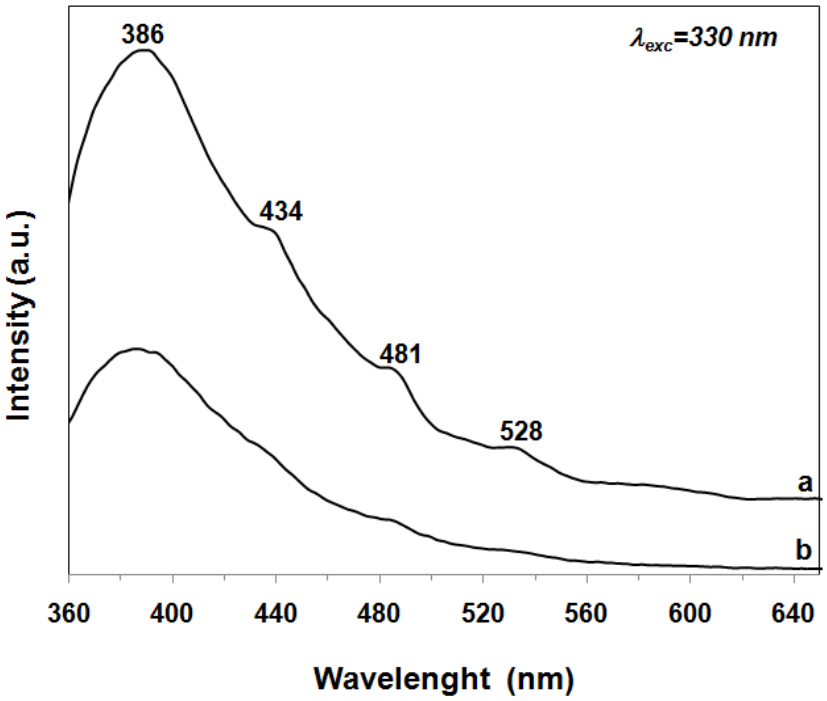

Figure 7.

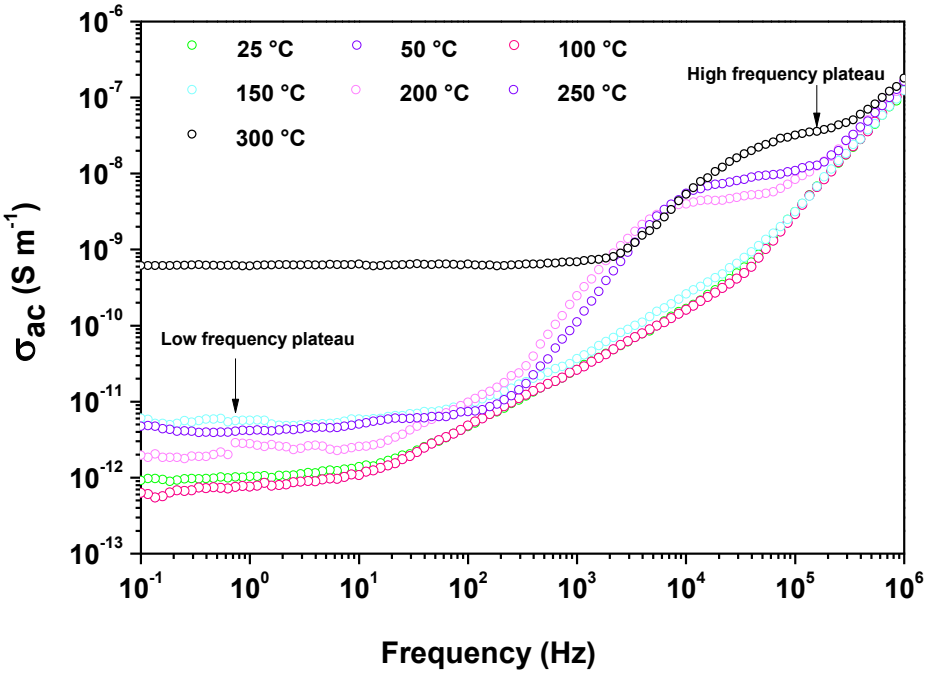

Figure 8.

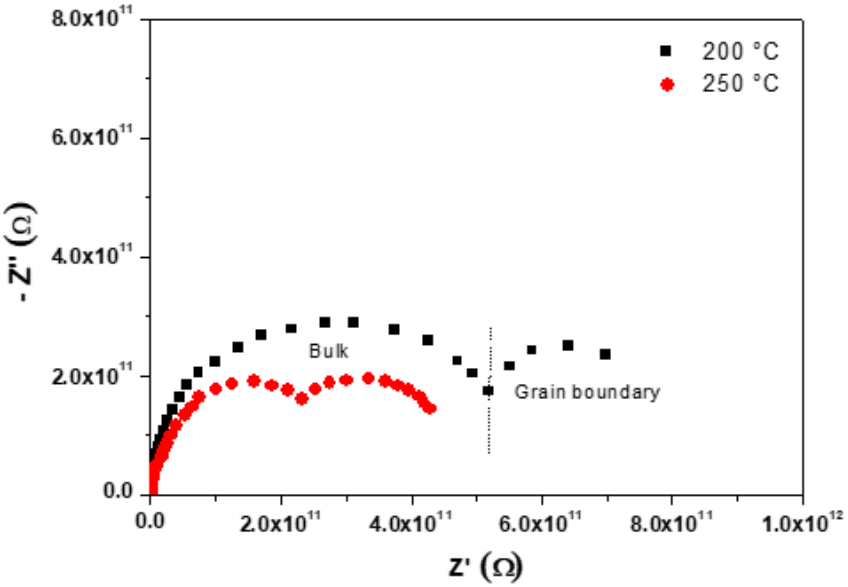
8.0x10^11
6.0x10^11
4.0x10^11
2.0x10^11
0.0
- Z'' (Ω)
0.0
2.0x10^11
4.0x10^11
6.0x10^11
8.0x10^11
1.0x10^12
Z' (Ω)
200 °C
250 °C
Bulk
Grain boundary

Figure 9.